Spin Hall Magnetoresistance in Metallic Bilayers

Junyeon Kim,[1] Peng Sheng,[1] Saburo Takahashi,[2] Seiji Mitani,[1] and Masamitsu Hayashi[1,*]
[1]National Institute for Materials Science, Tsukuba 305-0047, Japan
[2]Institute for Materials Research, Tohoku University, Sendai 980-8577, Japan
(Received 4 September 2015; revised manuscript received 8 February 2016; published 29 February 2016)

Spin Hall magnetoresistance (SMR) is studied in metallic bilayers that consist of a heavy metal (HM) layer and a ferromagnetic metal (FM) layer. We find a nearly tenfold increase of SMR in W/CoFeB compared to previously studied HM/ferromagnetic insulator systems. The SMR increases with decreasing temperature despite the negligible change in the W layer resistivity. A model is developed to account for the absorption of the longitudinal spin current to the FM layer, one of the key characteristics of a metallic ferromagnet. We find that the model not only quantitatively describes the HM layer thickness dependence of SMR, allowing accurate estimation of the spin Hall angle and the spin diffusion length of the HM layer, but also can account for the temperature dependence of SMR by assuming a temperature dependent spin polarization of the FM layer. These results illustrate the unique role a metallic ferromagnetic layer plays in defining spin transmission across the HM/FM interface.

DOI: 10.1103/PhysRevLett.116.097201

The resistance of a bilayer consisting of a heavy metal (HM) and a ferromagnetic insulator (FI) has been found to depend on the orientation of the magnetic layer [1–5]. As no current flows in the ferromagnetic insulator, identifying the origin of such magnetization direction dependent resistance, known as the magnetoresistance, has been one of the main focuses in this system. Among the various hypotheses proposed [6–12], many experimental results can be explained by a model [3,13,14] that invokes spin accumulation at the HM/FI interface. The model predicts that the size of the magnetoresistance scales with the square of the HM layer's spin Hall angle, a quantity that describes the degree of electron deflection with respect to the current flow due to the spin Hall effect. The observed magnetoresistance is thus commonly referred to as the spin Hall magnetoresistance (SMR).

The size of the spin Hall magnetoresistance has been reported to be small compared to the well-known anisotropic magnetoresistance [15] (AMR) in magnetic materials. Thus the effect of SMR on the transport properties of the system has been somewhat limited. Here we find large SMR, comparable to the size of AMR in Ni-based magnetic alloys, in metallic heterostructures consisting of a HM layer and a ferromagnetic metal (FM) layer, i.e., W/CoFeB. In addition to shunting current, one of the key characteristics of the FM layer is to absorb longitudinal spin current (spins pointing parallel to the FM magnetization direction). A spin transport model is developed to study the influence of this absorption on SMR. The model can quantitatively account for the HM layer thickness dependence of SMR and its temperature dependence. From these results, we find that the spin polarization of the ferromagnetic metal plays an important role in defining the SMR [1–5] and spin transport across HM/FM interfaces [7,16–19].

Films are deposited on thermally oxidized Si substrates using magnetron sputtering. We study two film structures with different heavy metal underlayers: Sub./d W/1 CoFeB/2 MgO/1 Ta and Sub./d Ta/1 CoFeB/2 MgO/1 Ta (unit in nanometer). Films are either postannealed at ~300 °C for 1 h prior to the device patterning processes (denoted as "annealed" hereafter) or patterned without the annealing treatment (denoted as "as dep."). Hall bars are patterned using optical lithography: the width (w) of the current flowing wire is ~10 μm and the distance (L) between voltage probes that measure the longitudinal resistance (R_{XX}) is ~25 μm. Definition of the coordinate axis is shown in Fig. 1(a). External magnetic field is applied along the x, y, and z axes, which we refer to as H_X, H_Y, and H_Z, respectively.

The magnetic properties of the films are shown in Figs. 1(b)–1(e). The saturated magnetic moment (M) divided by the volume (V) of the magnetic layer is plotted against the HM layer thickness in Figs. 1(b) and 1(c) for the W and Ta underlayer films. For all films, M/V is smaller than the nominal $Co_{20}Fe_{60}B_{20}$ saturation magnetization (M_S) ~1500 emu/cm^3 (Ref. [20]). This is likely due to the formation of a magnetic dead layer at the HM/FM interface [21]. We do not find any evidence of proximity induced magnetization, which may give rise to a magnetoresistance effect [2,8,9] different from the SMR, in Ta or W via magnetic moment measurements [22–26]. The magnetic anisotropy energy (K_{EFF}), shown in Figs. 1(d) and 1(e), illustrates the difference in K_{EFF} for films with and without annealing. For the annealed W underlayer films, K_{EFF} drops when d exceeds ~5 nm, which is due to the change in the structure of W [27,28]. K_{EFF} decreases when the Ta layer thickness increases for the annealed films, which we consider is partially due to an intermixing effect [21,29].

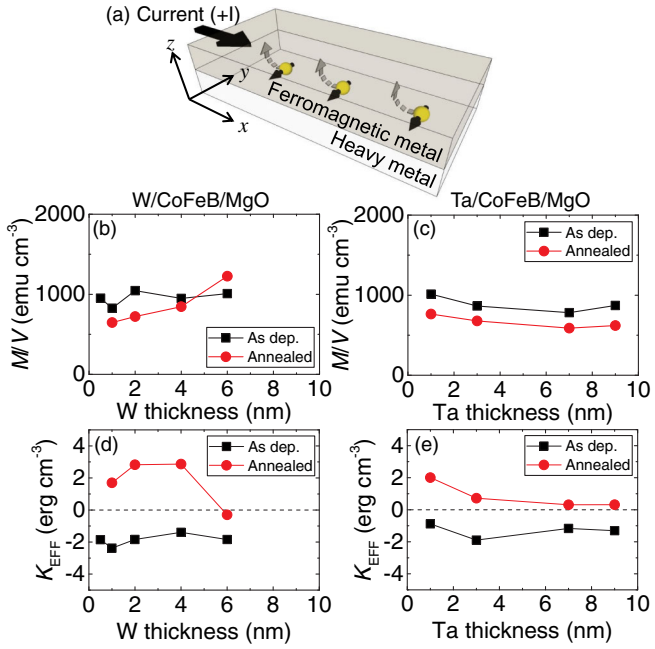

FIG. 1. (a) Schematic illustration of the system including the definition of the coordinate axis. (b),(c) Magnetic moment per unit volume (M/V) plotted as a function of the HM layer thickness for W/CoFeB/MgO (b) and Ta/CoFeB/MgO (c). (d),(e) The HM layer thickness dependence of the magnetic anisotropy energy (K_{EFF}) for W/CoFeB/MgO (d) and Ta/CoFeB/MgO (e). Black squares and red circles represent results of as deposited and annealed films, respectively.

Figure 2 shows typical field dependence of the longitudinal resistance for the as deposited (a) and annealed (b) W underlayer films. The longitudinal resistances measured against field orientations along the x, y, and z axes are defined as $R_{XX}(H_X)$, $R_{XX}(H_Y)$, and $R_{XX}(H_Z)$, respectively. The field dependence of R_{XX} is different for the as deposited and annealed films since the magnetic easy axis points along and normal to the film plane, respectively. At large field, however, the trend of $R_{XX}(H_{X,Y,Z})$ becomes similar; we find a large difference ($\sim$10 Ω) between $R_{XX}(H_Y)$ and $R_{XX}(H_Z)$, whereas the difference between $R_{XX}(H_X)$ and $R_{XX}(H_Z)$ is much smaller (less than 1 Ω). The former gives the spin Hall magnetoresistance [$\Delta R_{XX}^{\mathrm{SMR}} = R_{XX}(H_Y) - R_{XX}(H_Z)$] and the latter provides the anisotropic magnetoresistance [$\Delta R_{XX}^{\mathrm{AMR}} = R_{XX}(H_X) - R_{XX}(H_Z)$] (Refs. [3,14]).

The inverse of the heterostructure resistance when the magnetization is oriented along the z axis ($1/R_{XX}^0$) is plotted as a function of the HM layer thickness (d) in Figs. 3(a) and 3(b). The resistivity of the HM layer can be estimated from a linear line fit to the data, as shown by the solid lines. The obtained resistivity values are tabulated in Table I. The d dependence of the SMR ($\Delta R_{XX}^{\mathrm{SMR}}/R_{XX}^0$) is plotted in Figs. 3(c) and 3(d) for the W and Ta underlayer films (see Supplemental Material [30] for the details of how $\Delta R_{XX}^{\mathrm{SMR}}$ is obtained experimentally). For both samples, $|\Delta R_{XX}^{\mathrm{SMR}}/R_{XX}^0|$ takes a maximum at a certain underlayer

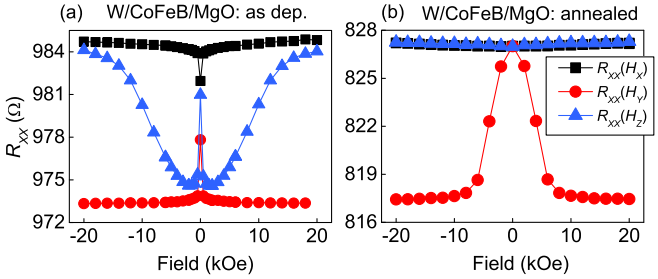

FIG. 2. (a),(b) The longitudinal resistance R_{XX} plotted against magnetic field oriented along the x axis (black squares), y axis (red circles), and z axis (blue triangles) for the as deposited (a) and annealed (b) W underlayer films. The W underlayer thickness is $\sim$3.3 (a) and $\sim$3.6 nm (b).

thickness ($d \sim 2$–3 nm). However, the magnitude of the maximum $|\Delta R_{XX}^{\mathrm{SMR}}/R_{XX}^0|$ is more than 10 times larger for the W underlayer films compared to that of the Ta underlayer films. Note that $|\Delta R_{XX}^{\mathrm{SMR}}/R_{XX}^0|$ drops when $d \sim 5$ nm for the W underlayer films. This drop coincides with the structural phase transition of W which is associated with a change in its resistivity [see Fig. 3(a)]. The large SMR also modifies the transverse component of the magnetoresistance [13,14] (typically referred to as the planar Hall resistance). The large planar Hall resistance previously found [28] in the W underlayer films is therefore due to the large SMR: see Supplemental Material [30] for HM layer thickness dependence of the transverse magnetoresistance.

In order to account for the SMR in metallic systems, we extend a model developed previously [3,13,14]. The spin Hall magnetoresistance of a HM/FM bilayer reads

$$\frac{\Delta R_{XX}^{\mathrm{SMR}}}{R_{XX}^0} \sim -\theta_{\mathrm{SH}}^2 \frac{\lambda_N}{d} \frac{\tanh^2(d/2\lambda_N)}{1+\xi} \times \left[\frac{g_R}{1 + g_R \coth(d/\lambda_N)} - \frac{g_F}{1 + g_F \coth(d/\lambda_N)} \right],$$
$$g_R \equiv 2\rho_N \lambda_N \mathrm{Re}[G_{\mathrm{MIX}}],$$
$$g_F \equiv \frac{(1-P^2)\rho_N \lambda_N}{\rho_F \lambda_F \coth(t_F/\lambda_F)}, \quad (1)$$

where ρ_N, λ_N, and θ_{SH} represent the resistivity, the spin diffusion length, and the spin Hall angle of the HM layer, respectively. G_{MIX} is the so-called spin mixing conductance [31–33] that defines the absorption of the transverse spin current (spins pointing orthogonal to the FM magnetization) impinging on the HM/magnetic layer interface [34]. t_F, ρ_F, λ_F, and P represent the thickness, resistivity, spin diffusion length, and the current spin polarization of the magnetic layer, respectively. $\xi \equiv (\rho_N t_F/\rho_F d)$ describes the current shunting effect into the magnetic layer. We assume the areal interface resistance [35] is negligible here for metallic interfaces.

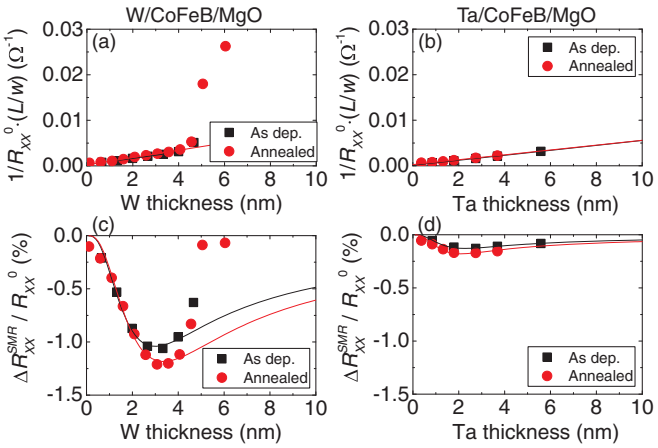

FIG. 3. (a),(b) Inverse of the film sheet resistance $1/R_{XX}{}^{0}$ (L/w) plotted as a function of HM layer thickness for W/CoFeB/MgO (a) and Ta/CoFeB/MgO (b). The solid lines are linear fit to the data. (c),(d) Spin Hall magnetoresistance $\Delta R_{XX}^{\mathrm{SMR}}/R_{XX}^{0}$ plotted against the HM layer thickness for W/CoFeB/MgO (c) and Ta/CoFeB/MgO (d). The solid lines show the fitting results using model B [$g_F \neq 0$ in Eq. (1)]. Model A [$g_F = 0$ in Eq. (1)] returns similar curves. Parameters used in the fitting are the following: Model A, $\mathrm{Re}[G_{\mathrm{MIX}}] = 10^{15}\ \Omega^{-1}\,\mathrm{cm}^{-2}$. Model B, $P = 0.72$, $\rho_F = 160\ \mu\Omega\,\mathrm{cm}$, $t_F = 1$ nm, $\lambda_F = 1$ nm, $\mathrm{Re}[G_{\mathrm{MIX}}] = 10^{15}\ \Omega^{-1}\,\mathrm{cm}^{-2}$. For both models, ρ_N is obtained from Table I. (a)–(d) Black squares and red circles represent results of as deposited and annealed films, respectively.

The first term in the square bracket of Eq. (1) has been derived to describe SMR in HM/FI systems: the peak value of the SMR vs d is primarily given by the product of the spin Hall angle (θ_{SH}) and $\mathrm{Re}[G_{\mathrm{MIX}}]$ which represents the degree of *transverse* spin current absorption. The second term in the square bracket characterizes the effect of a ferromagnetic metal which absorbs the *longitudinal* spin current. Because of this absorption, the SMR peak value decreases in HM/FM compared to that of HM/FI. The degree of reduction depends on spin polarization (P) of the ferromagnet metal: the smaller the P, the larger the reduction. Note that the absorption of the longitudinal spin current is the same when the FM magnetization is pointing parallel or antiparallel to the spin direction of the impinging spin current. This effect is thus different from the so-called "unidirectional SMR [18]" which originates from spin dependent scattering at the HM/FM interface. The thickness at which the SMR peak takes place is primarily determined by the spin diffusion length (λ_N) of the HM layer.

To study the effect of the longitudinal spin current absorption on the SMR, we compare the two limits of Eq. (1), which we refer to as models A and B hereafter. Model A neglects the longitudinal spin absorption and has been used to describe SMR in the HM/FI system. We set $g_F = 0$ in Eq. (1) to eliminate the second term in the square bracket. Model B takes into account the longitudinal spin absorption, a characteristic of the HM/FM system ($g_F \neq 0$). In model B we substitute $\rho_F \sim 160\ \mu\Omega\,\mathrm{cm}$ [28] and $P = 0.72$ [36] into Eq. (1). We fit the HM layer thickness dependence of SMR shown in Figs. 3(c) and 3(d) using the two models with $|\theta_{\mathrm{SH}}|$ and λ_N as the fitting parameters. For simplicity, a transparent interface for spin transmission is assumed, i.e., $\mathrm{Re}[G_{\mathrm{MIX}}] \to \infty$ ($\mathrm{Re}[G_{\mathrm{MIX}}] = 10^{15}\ \Omega^{-1}\,\mathrm{cm}^{-2}$ is assumed for the calculations). The fitted curves look similar for both models; results from model B are shown. $|\theta_{\mathrm{SH}}|$ and λ_N obtained from the fitting using both models are summarized in Table I. The estimated $|\theta_{\mathrm{SH}}|$ is larger for model B ($g_F \neq 0$) and agrees well with the values reported earlier using different techniques [27,37,38]. Note that the annealing treatment has little effect on $|\theta_{\mathrm{SH}}|$ even though it has a significant impact on the magnetic anisotropy of the system. As the anisotropy is defined at the CoFeB/MgO interface [39], these results show that the SMR is not significantly influenced by the state of the CoFeB/MgO interface even though the thickness of the CoFeB layer is small (1 nm thick).

When $\mathrm{Re}[G_{\mathrm{MIX}}]$ is reduced from its large limit, larger $|\theta_{\mathrm{SH}}|$ is required to fit the experimental results. Thus the values of $|\theta_{\mathrm{SH}}|$ tabulated in Table I are the lower limit of the estimation using the models employed here. For the W underlayer films with d larger than ~5 nm, $|\Delta R_{XX}^{\mathrm{SMR}}/R_{XX}^{0}|$ deviates from the fitted curve. We infer that this is due to the change in the spin Hall angle when the structure of W changes to the highly textured bcc phase [27].

The effect of the longitudinal spin absorption to the FM layer on the SMR is more pronounced in the temperature dependence of the SMR plotted in Fig. 4(a) for the

TABLE I. The resistivity (ρ_N), magnitude of the spin Hall angle ($|\theta_{\mathrm{SH}}|$) and the spin diffusion length (λ_N) of the heavy metal layer in HM/CoFeB/MgO evaluated at room temperature. ρ_N is obtained from the linear fitting shown in Figs. 3(a) and 3(b). $|\theta_{\mathrm{SH}}|$ and λ_N are obtained by the fitting shown in Figs. 3(c) and 3(d) using model A [$g_F = 0$ in Eq. (1)] and model B [$g_F \neq 0$ in Eq. (1)].

		Model A: HM/FI [$g_F = 0$]		Model B: HM/FM [$g_F \neq 0$]	
Film structure	ρ_N ($\mu\Omega$ cm)	$\lvert\theta_{\mathrm{SH}}\rvert$	λ_N (nm)	$\lvert\theta_{\mathrm{SH}}\rvert$	λ_N (nm)
W|CoFeB|MgO (annealed)	125	0.23	1.30	0.27	1.26
W|CoFeB|MgO (as dep.)	143	0.22	1.12	0.26	1.09
Ta|CoFeB|MgO (annealed)	187	0.10	0.72	0.11	0.70
Ta|CoFeB|MgO (as dep.)	183	0.08	0.79	0.10	0.77

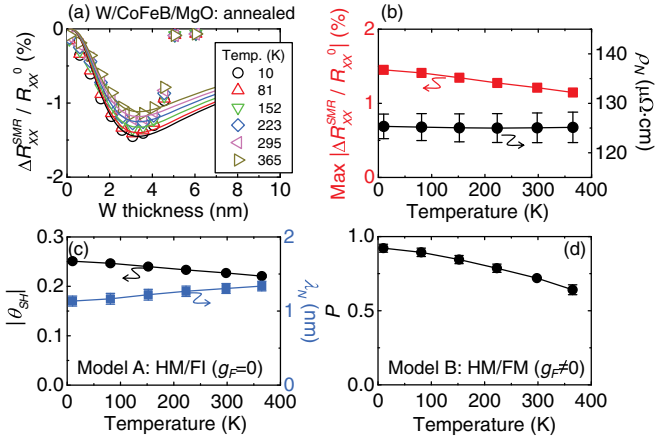

FIG. 4. (a) W layer thickness dependence of the spin Hall magnetoresistance $\Delta R_{XX}^{\mathrm{SMR}}/R_{XX}^{0}$ for the annealed W underlayer films measured at different temperatures. The solid lines show fitting results with model B. (b) The maximum $|\Delta R_{XX}^{\mathrm{SMR}}/R_{XX}^{0}|$ (red squares) and the resistivity (ρ_N) of the W underlayer (black circles) plotted as a function of measurement temperature. (c) Temperature dependence of the spin Hall angle (θ_{SH}) and the spin diffusion length (λ_N) of the W layer estimated from fitting the results of (a) using model A [$g_F = 0$ in Eq. (1)]. $\rho_N = 125\ \mu\Omega\,\mathrm{cm}$, $\mathrm{Re}[G_{\mathrm{MIX}}] = 10^{15}\ \Omega^{-1}\,\mathrm{cm}^{-2}$ are used in the fitting with model A. (d) Temperature dependence of the spin polarization (P) of the ferromagnetic layer obtained from fitting the results of (a) with model B [$g_F \neq 0$ in Eq. (1)]. $\rho_N = 125\ \mu\Omega\,\mathrm{cm}$, $|\theta_{\mathrm{SH}}| = 0.27$ and $\lambda_N = 1.26$ nm are fixed to their room temperature value, $\rho_F = 160\ \mu\Omega\,\mathrm{cm}$, $t_F = 1$ nm, $\lambda_F = 1$ nm, $\mathrm{Re}[G_{\mathrm{MIX}}] = 10^{15}\ \Omega^{-1}\,\mathrm{cm}^{-2}$ are assumed in the fitting with model B. The error bars indicate the fitting errors.

annealed W underlayer films. The peak amplitude of $|\Delta R_{XX}^{\mathrm{SMR}}/R_{XX}^{0}|$ increases as the temperature is decreased [Fig. 4(b), red squares]. In contrast, the resistivity of the W layer, estimated from the slope of $1/R_{XX}^{0}(L/w)$ vs d, shows almost no temperature dependence [Fig. 4(b), black circles]. The temperature dependence of SMR here is different from what has been reported for the HM/FI (Pt/YIG) system [40,41], in which the SMR decreases with decreasing temperature. To account for the change in the peak amplitude of $|\Delta R_{XX}^{\mathrm{SMR}}/R_{XX}^{0}|$ with temperature, we compare the two models described above.

In model A [$g_F = 0$ in Eq. (1)], the temperature dependent variables are λ_N, θ_{SH}, and $\mathrm{Re}[G_{\mathrm{MIX}}]$. For a transparent interface ($\mathrm{Re}[G_{\mathrm{MIX}}] \to \infty$), we show in Fig. 4(c) the changes in λ_N and θ_{SH} with temperature that give the best fit to the experimental data using model A. θ_{SH} increases and λ_N decreases with decreasing temperature. Although the temperature dependence of θ_{SH} can be accounted for if the spin Hall effect has an intrinsic origin [42], the change in λ_N with temperature is counterintuitive and inconsistent with the temperature dependence of the resistivity. It is possible to describe the temperature dependence of SMR with a temperature dependent $\mathrm{Re}[G_{\mathrm{MIX}}]$ and constant $|\theta_{\mathrm{SH}}|$ and λ_N. This will require the absolute value of $\mathrm{Re}[G_{\mathrm{MIX}}]$ to be small compared to what has been reported for metallic interfaces [16,43].

In contrast, model B [$g_F \neq 0$ in Eq. (1)] offers a better explanation on the SMR temperature dependence using reasonable values of $|\theta_{\mathrm{SH}}|$ and λ_N with a transparent interface. Given the negligible change of ρ_N with temperature, we assume that λ_N and θ_{SH} are temperature independent. The only parameter that changes with temperature is the spin polarization of the ferromagnet (P), which we set its room temperature value to ~0.72 [36,44]. Figure 4(d) shows the temperature dependence of P that gives the best fit to $|\Delta R_{XX}^{\mathrm{SMR}}/R_{XX}^{0}|$ vs d at different temperatures. Such change in the spin polarization with temperature is consistent with previous reports using direct measurements [45,46]. These results show that the longitudinal spin absorption to the FM layer can quantitatively describe the temperature dependence of SMR, giving an intuitive picture of spin transport across metallic interfaces.

We finally note that in metallic bilayer systems, the anomalous Hall effect (and/or the spin Hall effect) of the FM layer can influence the SMR. From the HM layer thickness dependence of the anomalous Hall resistance, we estimate the anomalous Hall angle (θ_{AH}) of the CoFeB layer to be within a range of ~0.02 to ~0.06 (see Supplemental Material [30]). Although such θ_{AH} will not significantly influence the results for the W underlayer films, it will impact the estimation of the spin Hall angle θ_{SH} for the Ta underlayer films: we consider θ_{SH} for Ta is overestimated due to the CoFeB anomalous Hall effect.

In summary, we have studied the spin Hall magnetoresistance in metallic bilayers. We find a large SMR in W/CoFeB, which increases with decreasing temperature. A model is developed to account for the longitudinal spin current absorption to the ferromagnetic metal (FM) layer, a key characteristic of metallic systems. The model can quantitatively describe the heavy metal (HM) layer thickness dependence and the temperature dependence of SMR. These results show that it is important to consider the longitudinal spin current absorption to the FM layer, a quantity that depends on the spin polarization of the FM, in describing spin transport across the HM/FM interface.

We thank K. Uchida and Y. Otani for helpful discussion, and H. Shimazu and J. Sinha for sample preparation. This work was partly supported by MEXT R&D Next-Generation Information Technology, the JSPS KAKENHI Grants No. 25706017, No. 25400337, No. 25247056, and No. 15H05702.

*hayashi.masamitsu@nims.go.jp

[1] M. Weiler, M. Althammer, F. D. Czeschka, H. Huebl, M. S. Wagner, M. Opel, I. M. Imort, G. Reiss, A. Thomas, R. Gross, and S. T. B. Goennenwein, Phys. Rev. Lett. **108**, 106602 (2012).

[2] S. Y. Huang, X. Fan, D. Qu, Y. P. Chen, W. G. Wang, J. Wu, T. Y. Chen, J. Q. Xiao, and C. L. Chien, Phys. Rev. Lett. **109**, 107204 (2012).

[3] H. Nakayama, M. Althammer, Y. T. Chen, K. Uchida, Y. Kajiwara, D. Kikuchi, T. Ohtani, S. Geprags, M. Opel, S. Takahashi, R. Gross, G. E. W. Bauer, S. T. B. Goennenwein, and E. Saitoh, Phys. Rev. Lett. **110**, 206601 (2013).

[4] C. Hahn, G. de Loubens, O. Klein, M. Viret, V. V. Naletov, and J. Ben Youssef, Phys. Rev. B **87**, 174417 (2013).

[5] N. Vlietstra, J. Shan, V. Castel, B. J. van Wees, and J. Ben Youssef, Phys. Rev. B **87**, 184421 (2013).

[6] M. I. Dyakonov, Phys. Rev. Lett. **99**, 126601 (2007).

[7] A. Kobs, S. Hesse, W. Kreuzpaintner, G. Winkler, D. Lott, P. Weinberger, A. Schreyer, and H. P. Oepen, Phys. Rev. Lett. **106**, 217207 (2011).

[8] Y. M. Lu, J. W. Cai, S. Y. Huang, D. Qu, B. F. Miao, and C. L. Chien, Phys. Rev. B **87**, 220409 (2013).

[9] B. F. Miao, S. Y. Huang, D. Qu, and C. L. Chien, Phys. Rev. Lett. **112**, 236601 (2014).

[10] T. Lin, C. Tang, H. M. Alyahayaei, and J. Shi, Phys. Rev. Lett. **113**, 037203 (2014).

[11] V. L. Grigoryan, W. Guo, G. E. W. Bauer, and J. Xiao, Phys. Rev. B **90**, 161412 (2014).

[12] J. X. Li, M. W. Jia, Z. Ding, J. H. Liang, Y. M. Luo, and Y. Z. Wu, Phys. Rev. B **90**, 214415 (2014).

[13] Y. T. Chen, S. Takahashi, H. Nakayama, M. Althammer, S. T. B. Goennenwein, E. Saitoh, and G. E. W. Bauer, Phys. Rev. B **87**, 144411 (2013).

[14] M. Althammer *et al.*, Phys. Rev. B **87**, 224401 (2013).

[15] T. R. McGuire and R. I. Potter, IEEE Trans. Magn. **11**, 1018 (1975).

[16] F. D. Czeschka, L. Dreher, M. S. Brandt, M. Weiler, M. Althammer, I. M. Imort, G. Reiss, A. Thomas, W. Schoch, W. Limmer, H. Huebl, R. Gross, and S. T. B. Goennenwein, Phys. Rev. Lett. **107**, 046601 (2011).

[17] J. C. Rojas-Sanchez, N. Reyren, P. Laczkowski, W. Savero, J. P. Attane, C. Deranlot, M. Jamet, J. M. George, L. Vila, and H. Jaffres, Phys. Rev. Lett. **112**, 106602 (2014).

[18] C. O. Avci, K. Garello, A. Ghosh, M. Gabureac, S. F. Alvarado, and P. Gambardella, Nat. Phys. **11**, 570 (2015).

[19] W. Zhang, W. Han, X. Jiang, S.-H. Yang, and S. S. P. Parkin, Nat. Phys. **11**, 496 (2015).

[20] R. M. Bozorth, *Ferromagnetism* (Wiley-IEEE Press, New York, 1993).

[21] J. Sinha, M. Hayashi, A. J. Kellock, S. Fukami, M. Yamanouchi, M. Sato, S. Ikeda, S. Mitani, S. H. Yang, S. S. P. Parkin, and H. Ohno, Appl. Phys. Lett. **102**, 242405 (2013).

[22] I. Galanakis, M. Alouani, and H. Dreyssé, Phys. Rev. B **62**, 3923 (2000).

[23] R. Tyer, G. van der Laan, W. M. Temmerman, Z. Szotek, and H. Ebert, Phys. Rev. B **67**, 104409 (2003).

[24] S. Emori and G. S. D. Beach, J. Appl. Phys. **110**, 033919 (2011).

[25] K. S. Ryu, S. H. Yang, L. Thomas, and S. S. P. Parkin, Nat. Commun. **5**, 3910 (2014).

[26] T. Ueno, J. Sinha, N. Inami, Y. Takeichi, S. Mitani, K. Ono, and M. Hayashi, Sci. Rep. **5**, 14858 (2015).

[27] C. F. Pai, L. Q. Liu, Y. Li, H. W. Tseng, D. C. Ralph, and R. A. Buhrman, Appl. Phys. Lett. **101**, 122404 (2012).

[28] J. Torrejon, J. Kim, J. Sinha, S. Mitani, M. Hayashi, M. Yamanouchi, and H. Ohno, Nat. Commun. **5**, 4655 (2014).

[29] J. Sinha, M. Gruber, M. Kodzuka, T. Ohkubo, S. Mitani, K. Hono, and M. Hayashi, J. Appl. Phys. **117**, 043913 (2015).

[30] See Supplemental Material at http://link.aps.org/supplemental/10.1103/PhysRevLett.116.097201 for details of the SMR measurement methods and supplemental experimental results and discussion.

[31] A. Brataas, Y. V. Nazarov, and G. E. W. Bauer, Phys. Rev. Lett. **84**, 2481 (2000).

[32] M. Weiler, M. Althammer, M. Schreier, J. Lotze, M. Pernpeintner, S. Meyer, H. Huebl, R. Gross, A. Kamra, J. Xiao, Y.-T. Chen, H. J. Jiao, G. E. W. Bauer, and S. T. B. Goennenwein, Phys. Rev. Lett. **111**, 176601 (2013).

[33] J. Kim, J. Sinha, S. Mitani, M. Hayashi, S. Takahashi, S. Maekawa, M. Yamanouchi, and H. Ohno, Phys. Rev. B **89**, 174424 (2014).

[34] M. D. Stiles and A. Zangwill, Phys. Rev. B **66**, 014407 (2002).

[35] S. Garzon, I. Zutic, and R. A. Webb, Phys. Rev. Lett. **94**, 176601 (2005).

[36] S. Fukami, T. Suzuki, Y. Nakatani, N. Ishiwata, M. Yamanouchi, S. Ikeda, N. Kasai, and H. Ohno, Appl. Phys. Lett. **98**, 082504 (2011).

[37] L. Liu, C.-F. Pai, Y. Li, H. W. Tseng, D. C. Ralph, and R. A. Buhrman, Science **336**, 555 (2012).

[38] H. L. Wang, C. H. Du, Y. Pu, R. Adur, P. C. Hammel, and F. Y. Yang, Phys. Rev. Lett. **112**, 197201 (2014).

[39] S. Ikeda, K. Miura, H. Yamamoto, K. Mizunuma, H. D. Gan, M. Endo, S. Kanai, J. Hayakawa, F. Matsukura, and H. Ohno, Nat. Mater. **9**, 721 (2010).

[40] S. Meyer, M. Althammer, S. Gepraegs, M. Opel, R. Gross, and S. T. B. Goennenwein, Appl. Phys. Lett. **104**, 242411 (2014).

[41] S. T. B. Goennenwein, R. Schlitz, M. Pernpeintner, K. Ganzhorn, M. Althammer, R. Gross, and H. Huebl, Appl. Phys. Lett. **107**, 172405 (2015).

[42] G. Y. Guo, S. Murakami, T. W. Chen, and N. Nagaosa, Phys. Rev. Lett. **100**, 096401 (2008).

[43] In Ref. [33], we describe the temperature dependence of the dampinglike and the fieldlike components of the spin Hall torque assuming a small $\mathrm{Re}[G_{\mathrm{MIX}}]$. It remains to be seen whether such a model is sufficient or other effects need to be taken into account to describe the current induced torques.

[44] S. X. Huang, T. Y. Chen, and C. L. Chien, Appl. Phys. Lett. **92**, 242509 (2008).

[45] M. Zhu, C. L. Dennis, and R. D. McMichael, Phys. Rev. B **81**, 140407 (2010).

[46] K. Ueda, T. Koyama, R. Hiramatsu, D. Chiba, S. Fukami, H. Tanigawa, T. Suzuki, N. Ohshima, N. Ishiwata, Y. Nakatani, K. Kobayashi, and T. Ono, Appl. Phys. Lett. **100**, 202407 (2012).